Cryogenics 143 (2024) 103926

Contents lists available at ScienceDirect

Cryogenics

journal homepage: www.elsevier.com/locate/cryogenics

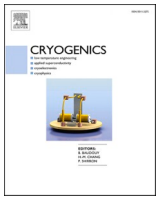

Modeling of cryogenic heated-tube flow boiling experiments of hydrogen and helium with the Generalized Fluid System Simulation Program

André LeClair [a,*], Michael Baldwin [a], Alok Majumdar [a], Jason Hartwig [b], Vishwanath Ganesan [c], Issam Mudawar [c]

[a] NASA/Marshall Space Flight Center, Huntsville, AL, USA
[b] NASA/Glenn Research Center, Cleveland, OH, USA
[c] Purdue University Boiling and Two-Phase Flow Laboratory (PU-BTPFL), West Lafayette, IN, USA

ARTICLE INFO

Keywords:
Boiling
Two-phase flow
Heat transfer coefficient correlation
Network flow analysis
Conjugate heat transfer
Liquid hydrogen
Liquid helium

ABSTRACT

Accurate modeling of cryogenic boiling heat transfer is vital for the development of extended-duration space missions. Such missions may require the transfer of cryogenic propellants from in-space storage depots or the cooling of nuclear reactors. Purdue University in collaboration with NASA has assembled a database of cryogenic flow boiling data points from steady-state heated-tube experiments dating back to 1959, which has been used to develop new flow boiling correlations specifically for cryogens. Computational models of several of these experiments have been constructed in the Generalized Fluid System Simulation Program (GFSSP), a network flow code developed at NASA's Marshall Space Flight Center. The new Purdue-developed universal correlations cover the full boiling curve: onset of nucleate boiling, nucleate boiling, critical heat flux, and film boiling. These correlations have been coded into GFSSP user subroutines. The fluids modeled in this study are liquid hydrogen and liquid helium. Predictions of local wall temperature and pressure drop are presented and compared to the test data.

1. Introduction

The combination of a flowing cryogenic fluid with large temperature differences between the surroundings and fluid implies that there will be complex flow boiling, heat transfer, and two-phase flow patterns. Accurate predictive tools for cryogenic two-phase flow boiling heat transfer and pressure drop are desired to design, analyze, and size efficient cryogenic transfer systems both on the ground and in microgravity. Penalties for poor models include increased safety factors, higher margins, and overall increases in cost. The use of flow boiling in a wide range of applications has pushed the development of so-called "universal correlations" [1–4] that would aid in the design and analysis of fluid transfer systems. Although these correlations covered a broad range of conditions for predicting heat flux and pressure drop, they did not specifically cover cryogenic fluids [5,6].

The two types of flow boiling encountered in cryogenic propellant transfer are quenching (or chill-down) and heating. In quenching, the initial wall temperature is much higher than the inlet bulk fluid temperature, and the fluid is used to cool the hot tube. Quenching is a transient process in which both the heat flux and wall temperature change with time. The heating configuration is a steady-state case where heating of the wall causes the fluid enthalpy to increase as it flows through the pipe. The heat transfer regimes that the fluid undergoes inside the pipe can include single-phase liquid convection until the onset of nucleate boiling, nucleate boiling until the critical heat flux point, and film boiling from the critical heat flux point until complete vaporization.

Correlations have been developed specifically for cryogenic flow boiling in the quenching configuration [7]. These correlations were tested in GFSSP and SINDA/FLUINT, and the results showed significant improvement in liquid nitrogen chill-down, and modest improvement in liquid hydrogen chill-down [8,9]. In the heating configuration, as in the case of the quenching configuration, comparison of heated tube cryogenic data with available heat transfer coefficient correlations has also shown that existing correlations do not accurately predict cryogenic heated tube data [6].

Accurate lumped node modeling of heated tube or steady state cryogenic flow is required for many space cryogenic transfer system applications. For example, after the initial chill-down of the transfer line that connects a refueling element or depot storage tank to a receiver

* Corresponding author at: M/S: ER43, NASA Marshall Space Flight Center, Huntsville, AL 35812, USA.
E-mail address: andre.c.leclair@nasa.gov (A. LeClair).

https://doi.org/10.1016/j.cryogenics.2024.103926
Received 18 April 2024; Received in revised form 31 July 2024; Accepted 15 August 2024
Available online 16 August 2024
0011-2275/Published by Elsevier Ltd.

Nomenclature

CHF	Critical Heat Flux, W/m^2
DB	Dittus-Boelter correlation
DFFB	Dispersed Flow Film Boiling
dP	Pressure Drop, Pa
FB	Film Boiling
g	Gravitational acceleration (9.81 m/s^2)
G	Mass Flux, kg/m^2-s
GFSSP	Generalized Fluid System Simulation Program
h	Heat transfer coefficient, W/m^2-K
HEM	Homogeneous Equilibrium Model for pressure drop
IAFB	Inverted Annular Film Boiling
LHe	Liquid Helium
LH_2	Liquid Hydrogen
MAPE	Mean Absolute Percentage Error
NB	Nucleate Boiling
ONB	Onset of Nucleate Boiling
Q_{DNB}	Critical heat flux by Departure from Nucleate Boiling mechanism, W/m^2
Q_{DRY}	Critical heat flux by Dryout mechanism, W/m^2
Q_{FLX}	Constant applied heat flux, W/m^2
Q_{MOD}	Applied heat flux modified to increase with axial distance, W/m^2
SFM	Separated Flow Model for pressure drop
SMAPE	Symmetric Mean Absolute Percentage Error
T_{sat}	Fluid saturation temperature, K
T_W	Wall temperature, K
x_e	Thermodynamic Equilibrium quality (vapor mass fraction based on enthalpy)
z	Axial distance from inlet, m or cm
z_{CHF}	Axial distance from inlet to critical point where NB transitions to FB, m or cm
z_{ONB}	Axial distance from inlet to Onset of Nucleate Boiling, m or cm

Subscripts

f	Saturated liquid
g	Saturated vapor
tp	Two-phase

Greek

α	Void fraction (vapor volume fraction)
Θ	Percentage of points within 30 % of test data; angle w.r.t. horizontal
ρ	Density, kg/m^3
φ	Percentage of points within 50 % of test data; blending parameter

tank, modeling of the steady state transfer is required to determine the amount of subcooled margin needed in the tank upstream. Another example is the transfer of liquid hydrogen from the nuclear thermal propulsion storage tank to a downstream reactor (after the initial chill-down transient); subcooled liquid hydrogen flows from the tank to the turbopumps, and the hydrogen must be single phase liquid when it reaches the pump inlet to avoid cavitation in the pump. Modeling of the steady state transfer is thus required to characterize vaporization of the fluid and design of the feed system.

Numerical modeling of flow boiling in a heated tube is challenging owing to the various boiling regimes and the two-phase nature of the flow. In many instances, two-phase flows can be modeled assuming the liquid and vapor are in thermal equilibrium and move with the same speed. With this so-called homogeneous equilibrium flow assumption [10], it is not necessary to solve for the separate conservation equations for mass, momentum, and energy for the liquid and vapor phases. A single set of conservation equations can be solved using the properties of the saturated liquid–vapor mixture.

There have been several investigations [8,11,12] where chill-down of cryogenic transfer lines has been numerically simulated by analyzing one-dimensional two-phase flow using a homogeneous equilibrium flow model. For these investigations, a general-purpose flow network code, GFSSP (Generalized Fluid System Simulation Program) [13], was used. GFSSP is a finite-volume based network flow analysis code developed at NASA/Marshall Space Flight Center. A reasonable comparison of numerical predictions with analytical solution [11] and experimental data for long [12] and short [8] transfer lines has been demonstrated.

Beginning in 2019, researchers at Purdue University, in collaboration with NASA Glenn Research Center, have worked to assemble a database of cryogenic boiling data from heated tube experiments in the literature. More than 9000 data points from 53 sources cover cryogenic fluids such as hydrogen, helium, neon, argon, nitrogen, and methane. The data points have been used to develop so-called universal cryogenic flow boiling correlations for the onset of nucleate boiling (ONB) [14], subcooled [14] and saturated [15] nucleate boiling (NB) heat transfer coefficient, critical heat flux (CHF) [16], film boiling (FB) heat transfer coefficient [17], and steady-state two-phase pressure drop [18].

Prior flow-boiling modeling programs in GFSSP have concentrated on modeling chill-down experiments. Because there is also a need to develop modeling capability for steady-state heat transfer in cryogenic transfer lines, for this investigation GFSSP has been used to develop numerical models of flow boiling in steady-state heated tube experiments. The new universal cryogenic flow boiling and two-phase pressure drop correlations have been added to GFSSP as Fortran user subroutines. These new correlations cover more boiling regimes than GFSSP's built-in boiling correlation, which is only for film boiling. The algorithm also includes logic to determine automatically the appropriate boiling regime. Predicted wall temperatures and pressure drop are compared to the experimental data to evaluate the performance of the new cryogenic flow boiling correlations against liquid hydrogen (LH_2) and liquid helium (LHe) heated tube experiments. A mean absolute percent error in the predicted absolute wall temperature of less than 30 % is targeted. The accuracy of the prediction of the location of critical heat flux is also studied, as there are many applications where it is vital to ensure that the flow does not enter the film boiling regime.

2. Experiments modeled

Three experimental data sets were modeled for this paper. Lewis et al. [19] conducted flow boiling experiments with LH_2 flowing upward in a heated vertical tube. The tube was 40.96 cm long, with an inner diameter of 1.4097 cm. The stainless-steel wall had a thickness of 0.089 cm. Outer wall temperatures were measured along the length of the pipe at 12 or 15 stations (depending on the test series). The inlet pressure and bulk fluid temperature of the LH_2 were measured near the inlet of the heated section. The 28 test runs simulated for this work cover inlet pressures of 207–355 kPa, mass fluxes of 4–12 kg/m^2-s, and heat fluxes of 29–57 kW/m^2.

Hendricks et al. [20] also conducted LH_2 experiments in a vertical tube. Depending on the test series, the tube material was either Inconel or stainless steel. In all cases, the heated test section was 60.96 cm long. Depending on the test, inner diameters varied 0.85–1.29 cm, and wall thicknesses varied 0.025–0.081 cm. Outer wall temperatures and fluid static pressures were measured at 12 stations along the length of the pipe. The inlet bulk fluid temperature of the LH_2 was measured near the inlet of the heated section. The 11 test runs modeled for this work cover inlet pressures of 616–1113 kPa, mass fluxes of 327–1438 kg/m^2-s, and

heat fluxes of 735–2092 kW/m^2.

Giarrantano et al. [21] conducted flow boiling experiments with LHe flowing downward in a vertical tube. The length of the test section was 10 cm, with an inner diameter of 0.213 cm. The stainless-steel wall had a thickness of 0.016 cm. Outer wall temperatures were measured at ten stations along the length of the pipe. The inlet pressure and bulk fluid temperature of the liquid helium were measured near the inlet. The ten test runs simulated for this work cover inlet pressures of 109–176 kPa, mass fluxes of 48–626 kg/m^2-s, and heat fluxes of 0.6–5 kW/m^2.

3. GFSSP model

GFSSP is a finite-volume flow network solver [13]. A fluid network is discretized into fluid nodes separated by branches. The conservation equations for mass and energy are solved in the fluid nodes to calculate pressures and enthalpies. The momentum equation is solved in the branches to calculate flow rates. Conjugate heat transfer may be added to a model with solid nodes and conductors. The solid nodes represent the mass of the pipe wall. The conductors represent convection from the wall to the fluid or conduction between solid nodes.

3.1. Model construction

Fig. 1 illustrates the GFSSP model of the Lewis LH_2 flow boiling experiment. The Hendricks and Giarrantano models are similar in construction but have different node spacing.

On the left side of the model, at the inlet boundary node, the user sets the inlet pressure equal to the reported test pressure. A user subroutine fixes the inlet enthalpy at the first internal node based on the reported inlet equilibrium quality entered by the user.

On the right side of the model, the user enters a guess value for the exit pressure in the outlet boundary node. GFSSP does not set flow rates; rather, it calculates the flow rate between boundary pressures. Since the exit boundary pressure is not known, the user enters the reported mass flux. A user subroutine then adjusts the exit boundary pressure until the required mass flux is calculated by the model. Another user subroutine overwrites GFSSP's built-in homogeneous pressure drop formulation with the universal cryogenic two-phase pressure drop correlations (see Section 3.2).

The test section is discretized into pipe branches. The branches have varying length, so that the fluid nodes are placed at the same axial location as the thermocouples measuring the wall temperature. The fluid nodes between the pipe branches are connected to solid nodes by fluid-to-solid conductors to represent convection from the pipe wall. The surface area of these conductors is based on the discretized length and inner diameter of the pipe branch just upstream of the conductor. A user subroutine calculates the heat transfer coefficient based on the universal cryogenic flow boiling correlations (see Section 3.3). Conductors are also placed between the solid nodes to represent axial conduction along the pipe wall.

Finally, the user can enter the location of the critical point z_{CHF} as estimated from the test data, or enter a negative value as a flag that the code should determine the location of z_{CHF} (see Section 3.3).

3.2. Pressure drop calculation

The consolidated cryogenic flow boiling database was used to develop two-phase pressure drop correlations [18]. This section provides a brief description of the formulation, which is treated more fully in [22].

Two models of pressure drop are provided in the user subroutine: a Homogeneous Equilibrium Model (HEM), and a Separated Flow Model (SFM). Each model contains three pressure drop terms: friction, gravity (if the flow is not horizontal), and acceleration.

The code initially assumes that the HEM is true. It calculates the frictional pressure drop that would occur if the flow were saturated liquid ($dP_{F,f}$) or saturated vapor ($dP_{F,g}$). Then it evaluates the frictional pressure with the HEM ($dP_{F,HEM}$). If the ratio in equation (1) below is less than twice the equilibrium quality, the HEM is verified as true. Otherwise, the code switches to the SFM. Segregation of the pressure drop test data into two groups, those which could be accurately modeled by the HEM and those which required the SFM, showed a clear dependence on the ratio in equation (1).

$$\frac{dP_{F,HEM} - dP_{F,f}}{dP_{F,g} - dP_{F,f}} \leq 2x_e \tag{1}$$

The friction term in the HEM is evaluated with the McAdams two-phase viscosity relation [23]. This is similar to a single-phase pressure drop, except that the code first calculates a two-phase density and two-phase viscosity. In the SFM, the friction term is a modification of the Lockhart-Martinelli approach [24]; however, the coefficients of the polynomial have been modified to fit better the data in the cryogenic flow boiling database [18,22].

The gravity term in both the HEM and SFM is based on the two-phase density evaluated by:

$$\rho_{tp} = \alpha\rho_g + (1-\alpha)\rho_f \tag{2}$$

where α is the void fraction given by:

$$\alpha = \left[1 + \frac{1-x_e}{x_e}\left(\frac{\rho_g}{\rho_f}\right)^n\right]^{-1} \tag{3}$$

For the HEM, the exponent n of the density ratio in equation (3) is equal to 1. For the SFM, n is 2/3, as formulated by Zivi [25]. The gravitational pressure drop is then calculated as a function of Θ, the angle with respect to the horizontal:

$$dP_G = g\rho_{tp}sin(\theta)dz \tag{4}$$

The acceleration term depends on the change in void fraction and equilibrium quality between nodes at stations z and $z+\Delta z$:

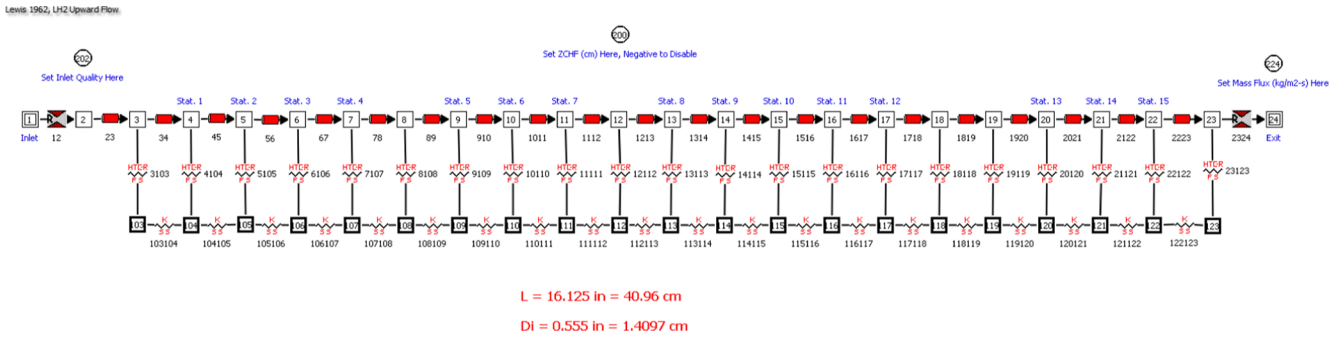

Fig. 1. GFSSP Model of Lewis LH_2 Flow Boiling Experiment.

$$dP_A = G^2\left[\left(\frac{x_{z+\Delta z}{}^2}{\rho_{g,z+\Delta z}\alpha_{z+\Delta z}} + \frac{(1-x_{z+\Delta z})^2}{\rho_{f,z+\Delta z}(1-\alpha_{z+\Delta z})}\right) - \frac{x_z{}^2}{\rho_{g,z}\alpha_z} + \frac{(1-x_z)^2}{\rho_{f,z}(1-\alpha_z)}\right] \quad (5)$$

As with the gravity term, the difference between the HEM and SFM void fractions in equation (5) is the value of the exponent n in equation (3).

The total pressure drop in each branch is the sum of the friction, gravity, and acceleration terms.

3.3. Heat transfer coefficient calculation

This section provides a brief description of the algorithm used to determine the heat transfer coefficients. The complete correlations are given in [14–17]. The methods by which the correlations are linked into a single boiling curve are described fully in [22].

In each iteration of the GFSSP solver, the code loops over each of the solid-to-fluid conductors representing convection heat transfer. The user subroutine begins by searching along the length of the test section for the axial location of the onset of nucleate boiling (ONB) and the critical point (z_{CHF}) where the boiling regime changes from nucleate boiling (NB) to film boiling (FB).

To determine ONB, at each node the code calculates what the convection coefficient would be if the fluid were single-phase saturated liquid, using the Dittus-Boelter correlation. Using this convection coefficient and the known heat flux, a notional wall temperature is evaluated. Then the wall temperature required for ONB [14,22] is evaluated by:

$$T_{w,ONB} = T_{sat} + 30.65\left(\frac{Q_{FLX}}{10^6}\right)^{0.5} exp\left(-\frac{P}{8.7*10^6}\right) \quad (6)$$

where the known applied heat flux Q_{FLX} is in units of W/m^2 and pressure P is in Pa. The first node where the notional single-phase wall temperature is greater than $T_{w,ONB}$ becomes the location for z_{ONB}.

To determine the critical point z_{CHF}, at each node the code evaluates two correlations for critical heat flux [16,22]. The first correlation represents the mechanism of Departure from Nucleate Boiling (DNB). The second correlation represents dryout. The critical point, z_{CHF}, occurs where there is an intersection between the Q_{DNB} or Q_{DRY} curves and the known applied heat flux, Q_{FLX}. An additional constraint is that the Q_{DNB} curve must intersect where the Zivi void fraction from Equation (3) is less than 0.6, and the Q_{DRY} curve must intersect where the Zivi void fraction is greater than 0.6.

In some cases there can be an ambiguity, where both the Q_{DNB} and Q_{DRY} curves intersect the Q_{FLX} curve, and both meet the void fraction criterion. When this occurs, the location of the Q_{DRY} intersection is taken as z_{CHF}. The consequences of this practice are discussed in the Results section.

Fig. 2 shows that the Q_{DNB} and Q_{DRY} curves have an asymptotically decreasing trend as they proceed along the axial length. In some cases, the curves never intersect the Q_{FLX} curve but rather plateau at a value slightly above Q_{FLX}. Owing to the asymptotic nature of the Q_{DNB} and Q_{DRY} curves, it is only at the far end of the heated length that such a scenario occurs. Thus, the user has the option of checking for intersection with a modified curve:

$$Q_{MOD} = Q_{FLX}\left[1 + a\left(\frac{z}{L}\right)^b\right] \quad (7)$$

For this study the values of a and b were 0.25 and 2, respectively. These values are chosen such that Q_{FLX}, instead of following a constant trend line, shows a gradual rise only at the far end of the heated length with the limiting condition of $Q_{MOD} = Q_{FLX}$ at $z = 0$ and $Q_{MOD} = 1.25\ Q_{FLX}$ at $z = 1$. This is done to account for the uncertainty in the Q_{DNB} and Q_{DRY} curves, estimated at 23–28 % in [16], and to improve the odds of predicting z_{CHF} within the heated length when the Q_{DNB} and Q_{DRY} curves tend to plateau. Since this will trigger the change to the FB regime and lead to higher predicted wall temperatures, for many applications this is a conservative approach.

At nodes between z_{ONB} and z_{CHF} the heat transfer coefficient is evaluated from one of two nucleate boiling correlations [15,22]. The nominal correlation covers nucleate boiling for the subcooled and saturated states. An alternative correlation is available for cases with high inlet quality. The latter occurs when the distance between the current axial location and the location upstream of the inlet where the fluid initially became saturated ($x_e = 0$) is greater than 1.1 times the total test section length.

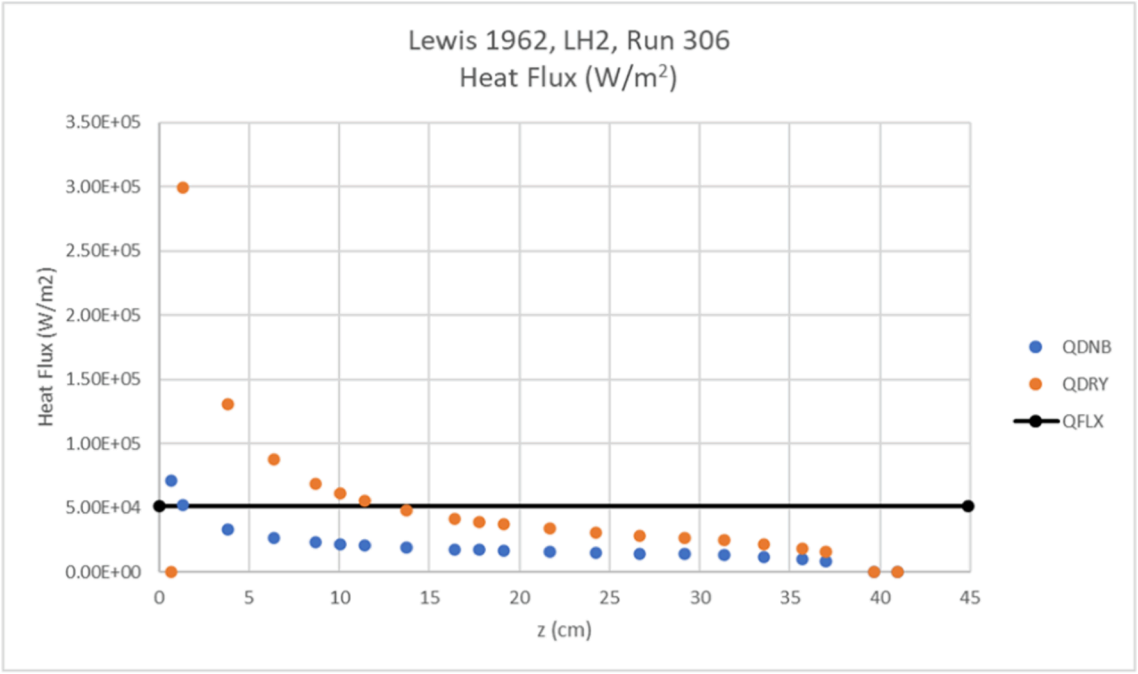

Fig. 2. Heat flux curves for Lewis Run 306.

At nodes after z_{CHF} the heat transfer coefficient is evaluated from one of several film boiling correlations [17,22]. One of two correlations is used for dispersed flow film boiling (DFFB), depending on whether the fluid is saturated or superheated. Another correlation is available for inverted annular film boiling (IAFB), covering both the saturated and superheated phases. These correlations depend on the equilibrium quality (based on the enthalpy of the node). A DFFB correlation based on actual quality (based on the masses of liquid and vapor) is also available but was not used in this study.

To determine whether to use DFFB or IAFB, the code initially assumes that DFFB is true and calculates the heat transfer coefficient, which is used with the known applied heat flux to calculate a notional wall temperature T_w. The code also calculates what the heat transfer coefficient would be if the Dittus-Boelter correlation were applied using saturated vapor properties, and this is used to calculate a notional wall temperature $T_{W,DB,g,e}$. The ratio of the degrees of superheat between these two wall temperatures is called ΔT^*.

$$\Delta T^* = \frac{T_w - T_{sat}}{T_{W,DB,g,e} - T_{sat}} \tag{8}$$

As determined by data segregation in [17], if the ratio ΔT^* is greater than or equal to 1.0, then DFFB is confirmed. If it is less than 1.0, then the code switches to the IAFB correlation. Note that it is possible to have IAFB for a few nodes in a model, before switching to DFFB.

At this time, there is no correlation for subcooled film boiling. As a placeholder, this study applied the form of the IAFB correlation evaluated with subcooled properties. The consequences of this practice will be discussed in the Results section.

It was observed that the predicted wall temperatures in the transition region immediately after z_{CHF} were often much higher than test data. This is due to the fact that the correlations were developed to produce an estimate of the post-CHF wall temperature that would be conservative from an engineering perspective (higher temperature). An ad hoc method of modeling the region of transition between NB and FB was devised. This method creates a patched heat transfer coefficient in the post-z_{CHF} region that uses a modified harmonic mean of the last pre-z_{CHF} value of NB heat transfer coefficient and the locally evaluated FB heat transfer coefficient.

$$\frac{1}{h_{tp,patched}} = \frac{1}{h_{tp,pre-CHF}} + \frac{1+\tanh(\varphi(z-z_{CHF}))}{2}\left(\frac{1}{h_{tp,post-CHF}} - \frac{1}{h_{tp,pre-CHF}}\right) \tag{9}$$

Note that as the axial distance z increases, the hyperbolic tangent function goes to 1.0, so that the NB heat transfer coefficient is removed from the blending. For this study, the smoothing parameter φ had a value of 5 m^{-1} for all runs.

When the critical point z_{CHF} was determined to be exactly at the inlet, so that there was no nucleate boiling upstream, the blending function was disabled.

4. Results & discussion

In this section are shown the results of models of selected runs from the three experimental cases. Predicted wall temperatures are compared to the reported measured values. In order to evaluate more clearly the performance of the NB and FB correlations, each experimental run was modeled twice: once where the code searched for z_{CHF}, and once with z_{CHF} fixed at the experimentally observed location, so that all points would be modeled in the correct boiling regime. This allows for an apples-to-apples comparison of pre-CHF test data to pre-CHF model predictions, and post-CHF test data to post-CHF model prediction.

Parity plots of all points are presented to illustrate the percentage of predicted wall temperatures that fall within ±30 % (Θ) or ±50 % (φ) of the measured values. Average errors are reported as the Mean Absolute Percentage Error (MAPE) and the Symmetric Mean Absolute Percentage Error (SMAPE). The MAPE is calculated as:

$$MAPE = \frac{100\%}{N}\sum\frac{|T_{w,pred} - T_{w,meas}|}{T_{w,meas}} \tag{10}$$

The SMAPE compensates for the fact that with the MAPE under-predictions of wall temperature can never be greater than 100 %, but over-predictions are limitless. The SMAPE is calculated as:

$$SMAPE = \frac{100\%}{N}\sum\frac{|T_{w,pred} - T_{w,meas}|}{\frac{1}{2}\left(|T_{w,pred}| + |T_{w,meas}|\right)} \tag{11}$$

The error in the location of z_{CHF} is also calculated when it is reported. However, because z_{CHF} may be zero when the critical heat flux point is at the inlet of the test section, the denominator is modified to normalize the absolute error by the overall length of the heated test section.

$$MAPE(Z_{CHF}) = \frac{100\%}{N}\sum\frac{|Z_{CHF,pred} - Z_{CHF,meas}|}{L} \tag{12}$$

4.1. Lewis et al. LH_2 (1962)

Figs. 2–3 illustrate the model output for Lewis Run 306. Run numbers correspond to those given in Table II(a) of [19]. For this run, the inlet pressure was 331 kPa. The mass flux was 10.8 kg/m^2-s, and the heat flux was 51.7 kW/m^2.

Fig. 2 plots the critical heat flux curves as functions of axial distance for Run 306. There is an intersection of the known applied heat flux (Q_{FLX}) with the Departure from Nucleate Boiling (Q_{DNB}) curve at 2 cm. However, there is also an intersection with the Dryout (Q_{DRY}) curve at 12.3 cm. As discussed in Section 3.3, when there is an ambiguity, the code logic chooses the Q_{DRY} intersection to be the critical point z_{CHF}. Lewis et al. report the observed z_{CHF} to be 10.2 cm.

Fig. 3 plots the measured and predicted wall temperatures for Lewis Run 306 when the code determined z_{CHF} at 12.3 cm. There is generally good agreement in both the NB and FB regimes. The largest error occurs at 11.4 cm, where the model used a NB correlation when a FB correlation would have been applied if z_{CHF} were more closely determined.

Fig. 4 plots the critical heat flux curves for Run 146. For this run, the inlet pressure was 352 kPa. The mass flux was 14.8 kg/m^2-s, and the heat flux was 59.0 kW/m^2. As with Run 306, there are two possible intersections of the Q_{DNB} and Q_{DRY} curves with the known applied Q_{FLX}. The code selects dryout and determines z_{CHF} at 13.1 cm. The measured wall temperatures indicate that the critical point lies somewhere upstream of the first thermocouple station at 1.3 cm (therefore $z_{CHF} \approx 0$ cm). In this instance, it would have been better to choose the Q_{DNB} intersection at 1.5 cm.

Fig. 5 shows the measured and predicted wall temperatures for Lewis Run 146 when the code incorrectly determined z_{CHF} at 13.1 cm. Note that there is significant error at the first five thermocouple stations, because the code has applied NB correlations instead of FB correlations.

For Run 146, where the critical point lies somewhere between the inlet and first thermocouple station at 1.3 cm, the model was re-run with z_{CHF} fixed at 0.65 cm. The results of this run are plotted in Fig. 6. The MAPE is decreased from 38 % when the code found z_{CHF} to 27 % when z_{CHF} was fixed so that all nodes at thermocouple stations were correctly placed in the FB regime.

Since Run 146 includes only wall temperatures in the FB regime, it is an ideal candidate for comparing the new universal cryogenic flow boiling correlations with the Miropolskii correlation, a film boiling correlation based on water experiments [26]. The Miropolskii correlation is built into GFSSP, which does not have a built-in nucleate boiling or critical heat flux correlation. Fig. 7 plots the predicted wall temperatures with the Miropolskii correlation in comparison with the new cryogenic flow boiling correlations when the code determined z_{CHF} at 13.1 cm. The MAPE with the Miropolskii correlation was 64 %, compared to 38 % with the new correlations.

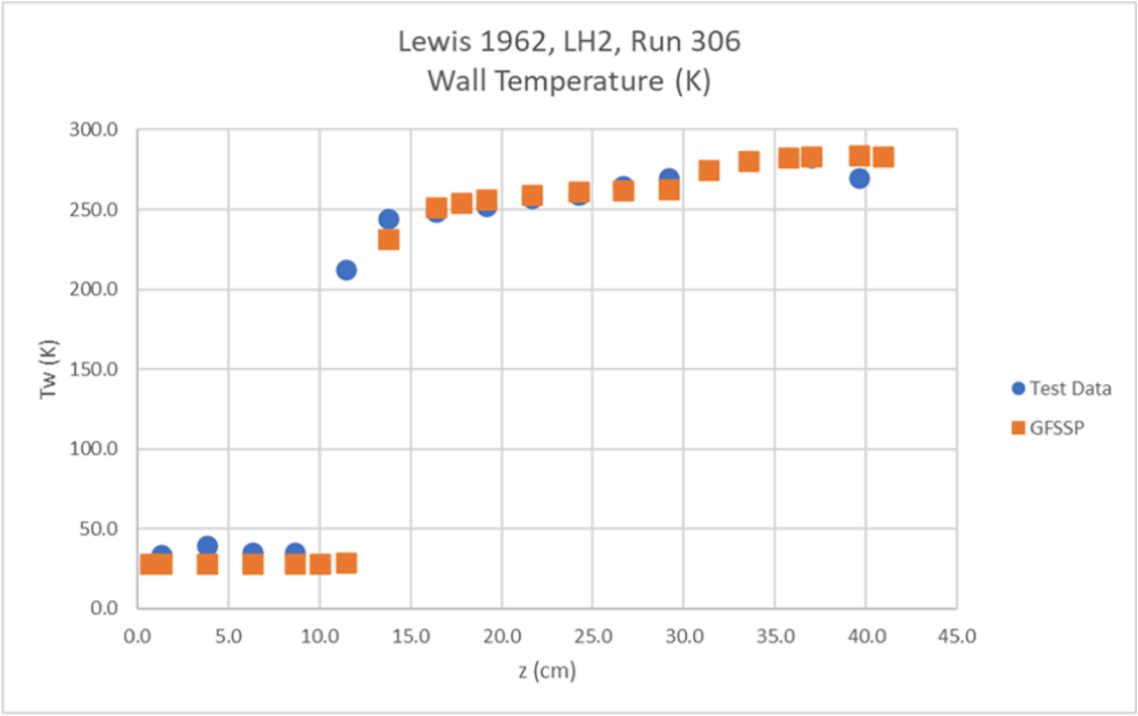

Fig. 3. Measured and predicted wall temperatures for Lewis Run 306, when the code determines z_{CHF}.

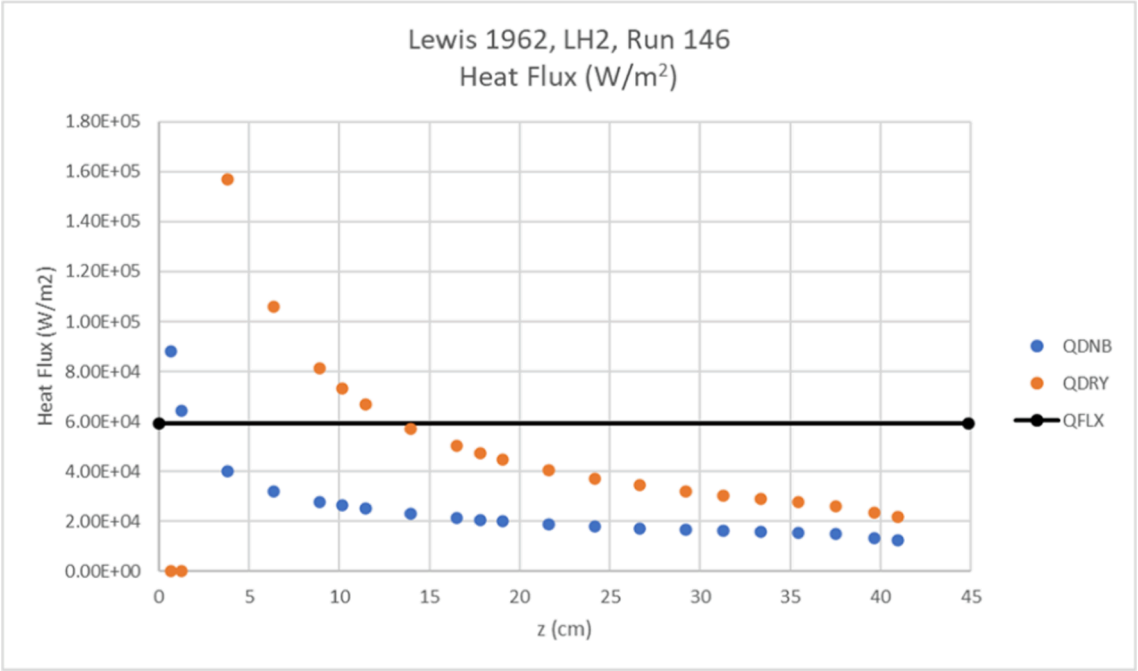

Fig. 4. Heat flux curves for Lewis Run 146.

Fig. 8 is a parity plot of all 368 wall temperatures from the 28 Lewis LH_2 runs modeled when the code searched for z_{CHF}. Ideally, the points should fall on the solid black line. The dashed black line indicates an error of ±30 %; the dotted line, ±50 %.

In Fig. 8, the MAPE is 46.6 %. The SMAPE is also calculated as 58.0 %. For the Lewis LH_2 runs when the code determines z_{CHF}, 61.1 % of the predicted wall temperatures fall within 30 % of the measured wall temperatures (Θ), and 66.3 % fall within 50 % (φ).

Fig. 8 shows that most of the large errors in prediction occur along the bottom of the plot, where the wall temperatures were incorrectly evaluated in the NB regime instead of the FB regime. These occur when the code determines z_{CHF} to be downstream of the actual critical point.

Fig. 9 is a parity plot of the Lewis LH_2 runs when z_{CHF} was fixed. Note that Lewis reported the location of z_{CHF} in only 8 of the 28 runs. For the remaining twenty, it is only known that z_{CHF} lies between the inlet and the first thermocouple at 1.3 cm. For these runs, z_{CHF} was fixed at 0.65 cm. It is seen that when z_{CHF} is fixed, the MAPE decreases from 46.6 % to 30.4 %. The percentage of predicted wall temperatures that fall within

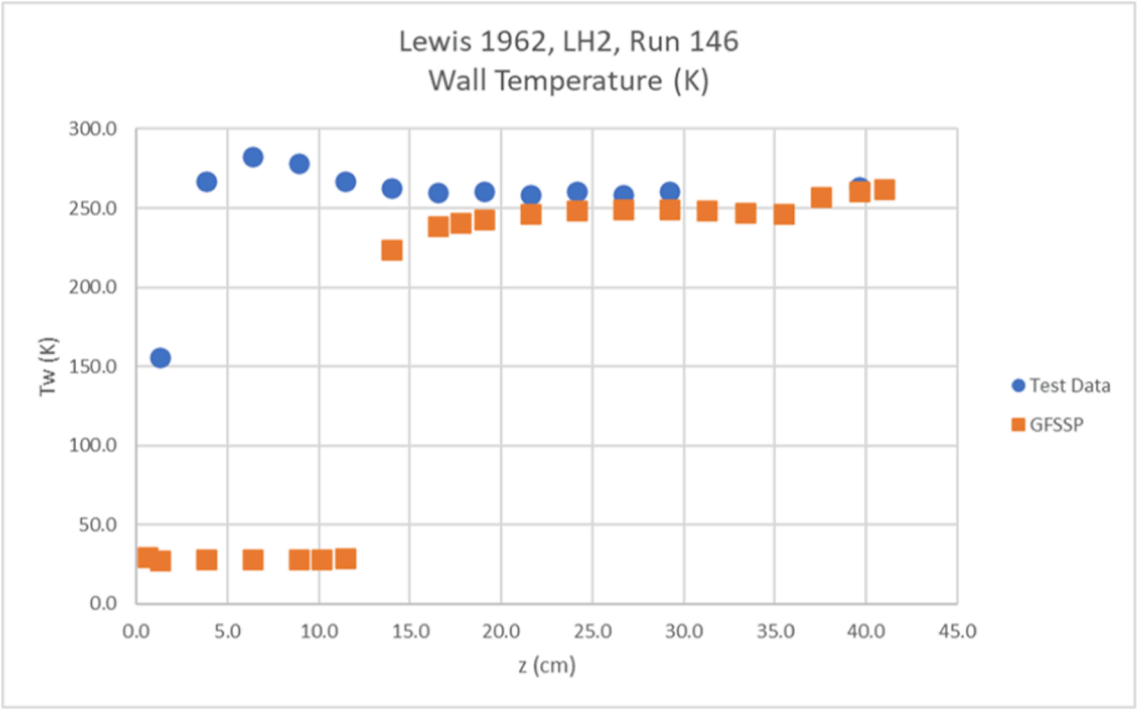

Fig. 5. Measured and predicted wall temperatures for Lewis Run 146, when the code determines z_{CHF}.

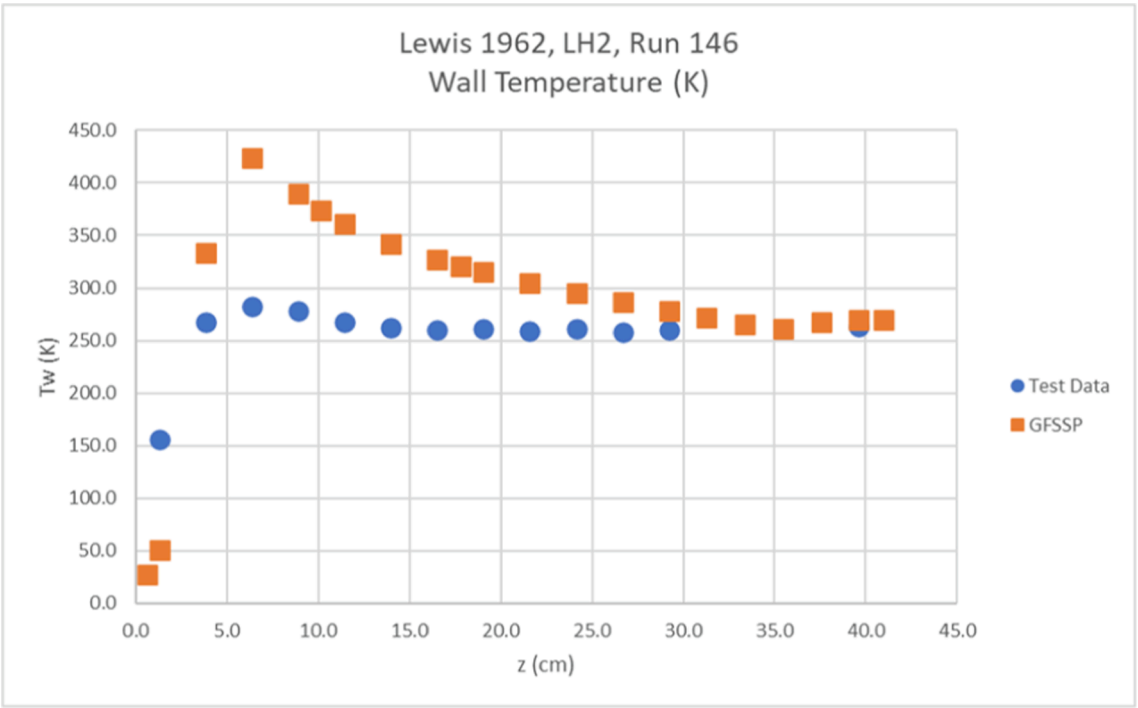

Fig. 6. Measured and predicted wall temperatures for Lewis Run 146, when z_{CHF} is fixed at 0.65 cm.

50 % of the test data increases from 66.3 % to 81.8 %. In general, when z_{CHF} is fixed, the Lewis LH_2 wall temperatures are more likely to be over-predicted than under-predicted.

Fig. 10 is a parity plot of the Lewis LH_2 runs when z_{CHF} is fixed, showing only the 35 measured wall temperatures that fall in the NB regime. The MAPE is just 18.4 %, and 88.6 % of the predicted wall temperatures fall within 30 % of the measured values. Note that there are four outliers where the code over-predicted the wall temperatures. These outliers have suspicious measured wall temperatures that are colder than the fluid inlet temperature.

Fig. 11 is a parity plot of the Lewis LH_2 runs when z_{CHF} is fixed, showing only the 333 measured wall temperatures that fall in the FB regime. The MAPE is 31.7 %, and 63.4 % of the predicted wall temperatures fall within 30 % of the measured values. The FB correlations appear more likely to over-predict the wall temperatures than to under-predict.

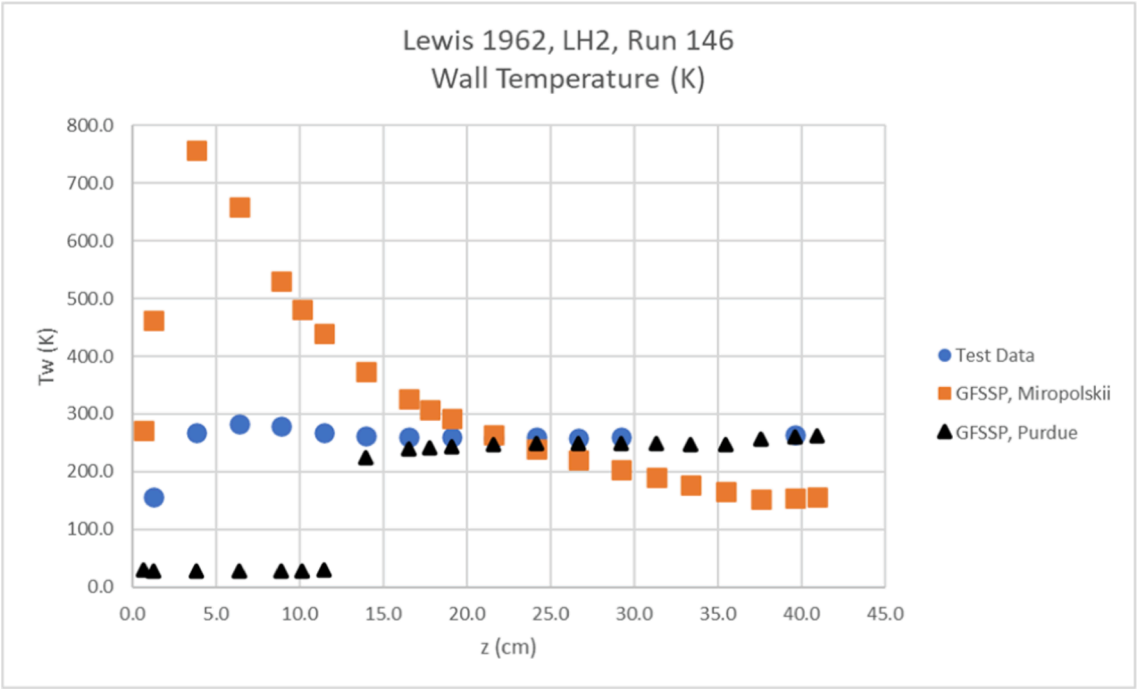

Fig. 7. Measured and predicted wall temperatures for Lewis Run 146 comparing the Miropolskii correlation with the Purdue universal cryogenic flow boiling correlations.

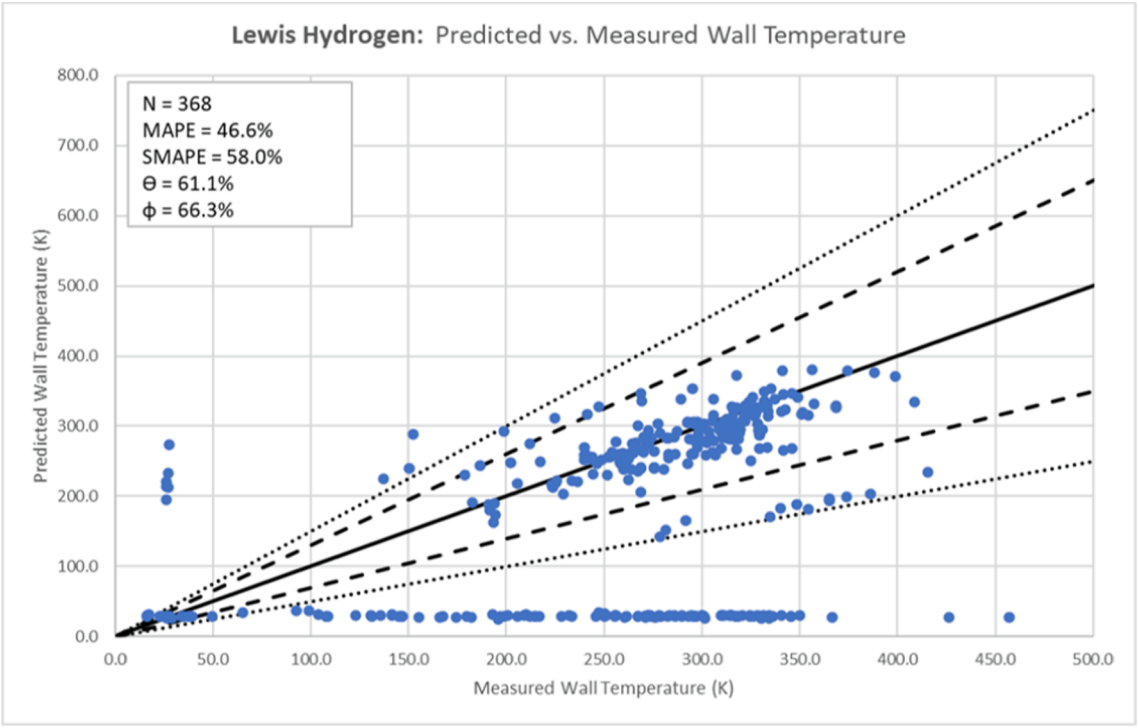

Fig. 8. Parity plot of all Lewis LH_2 runs when code searches for Z_{CHF}.

Fig. 12 is a parity plot comparing the predicted and reported locations of the critical point z_{CHF} for the 28 Lewis LH_2 runs. It is seen that the critical point is more likely to be reported downstream than upstream of the actual location. This accounts for the large number of points in Fig. 8 where the wall temperatures were incorrectly evaluated in the NB regime instead of FB. The mean absolute error in z_{CHF} was 25 % of the overall test section length of 40.96 cm.

4.2. *Hendricks et al. LH_2 (1966)*

Figs. 13–15 illustrate the model output for Hendricks Run 1_1146. Run numbers correspond to Tables III and IV of [20]. For this run, the inlet pressure was 760 kPa. The mass flux was 327 kg/m^2-s, and the heat flux was 1190 kW/m^2.

Fig. 13 plots the critical heat flux curves as functions of axial distance

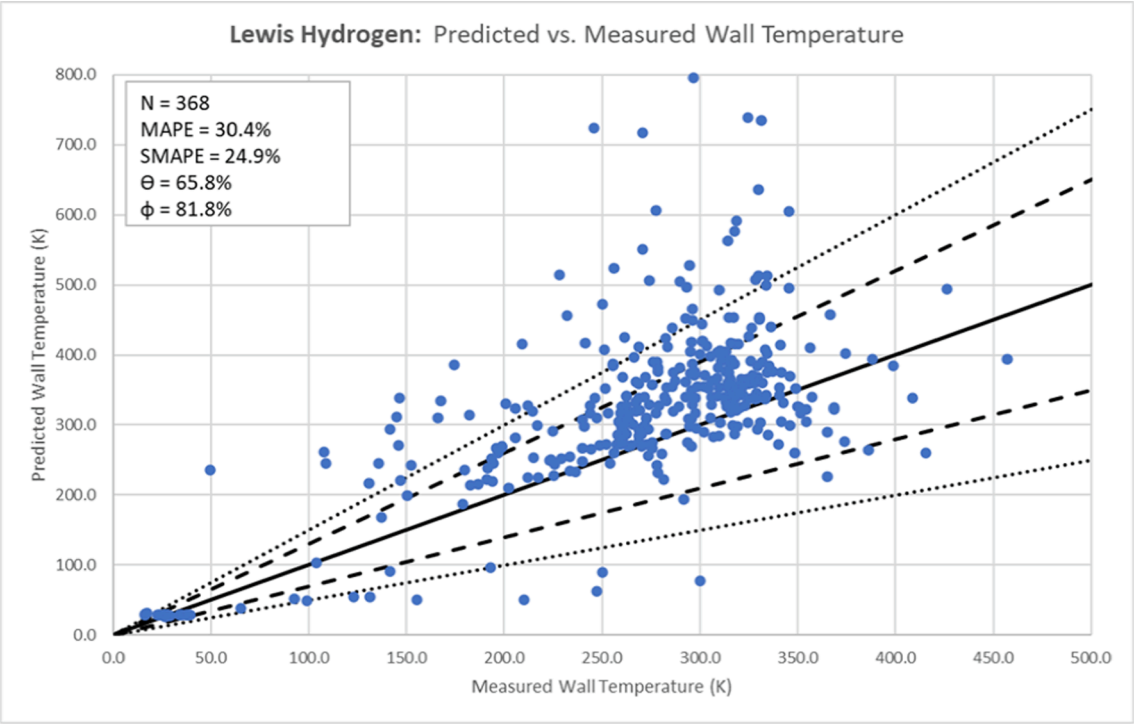

Fig. 9. Parity plot of all Lewis LH_2 runs when z_{CHF} is fixed at observed value.

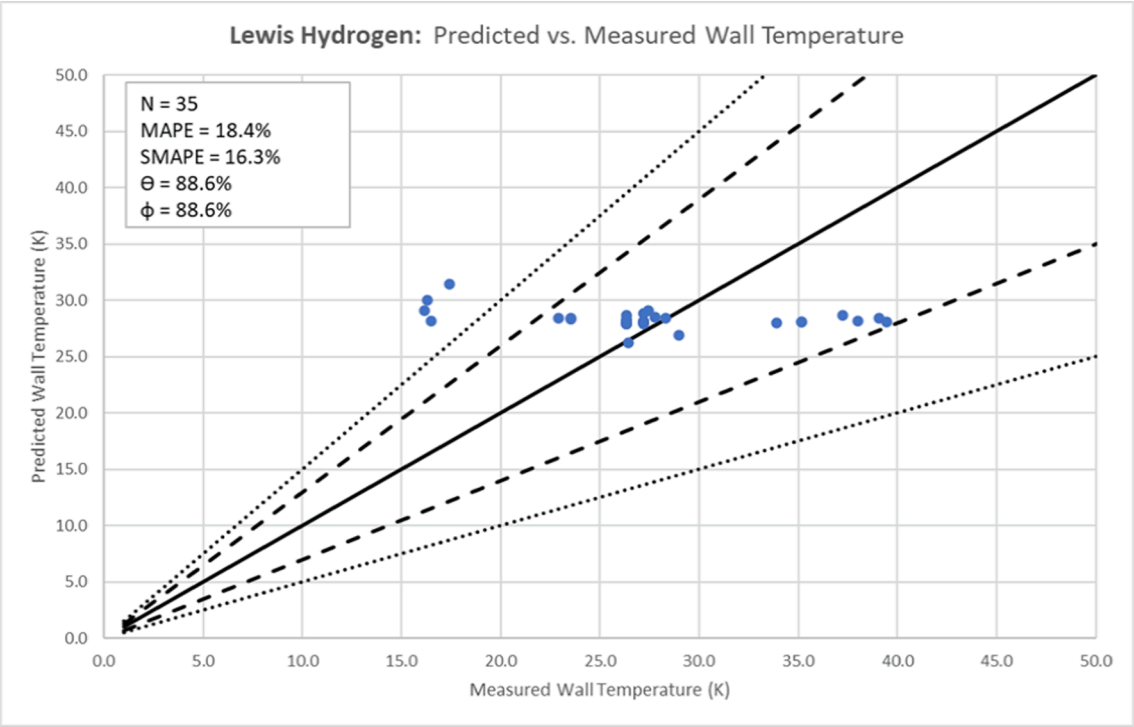

Fig. 10. Parity plot of NB regime points for Lewis LH_2 runs when z_{CHF} is fixed at observed value.

for Run 1_1146. Note that the known applied heat flux is greater than either the Q_{DNB} or Q_{DRY} curves, even at the inlet. Therefore, the code sets z_{CHF} at the inlet and the FB correlations are applied everywhere, with no blending function.

Fig. 14 plots the measured and predicted wall temperatures for Lewis Run 1_1146 when the code determined z_{CHF} at the inlet. Wall temperatures are generally under-predicted, except near the inlet when the FB correlations tend to produce low values of heat transfer coefficient at low qualities. Note the very low temperature predicted at 0.1 cm. This is not in the NB regime. Rather, the code is in the sub-cooled FB regime, for which there is not yet a new flow boiling correlation. As stated in Section 3.3, the superheated IAFB correlation, using subcooled properties, was substituted in this regime.

Fig. 15 plots the measured and predicted pressures along the axial

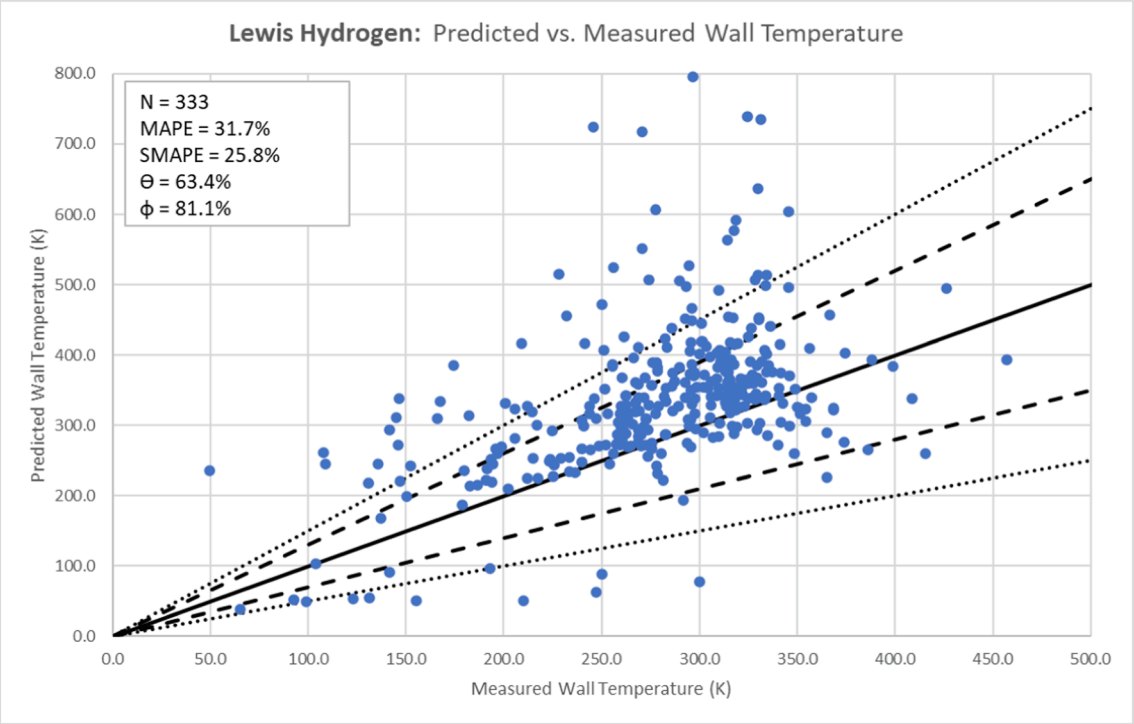

Fig. 11. Parity plot of FB regime points for Lewis LH_2 runs when z_{CHF} is fixed at observed value.

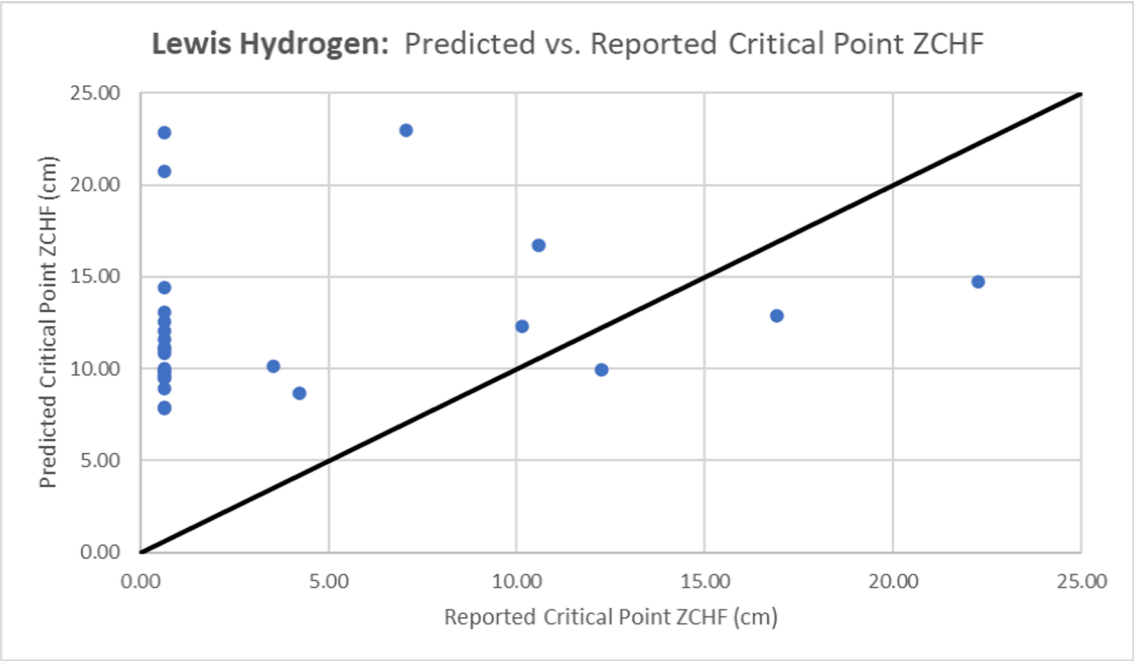

Fig. 12. Parity plot of predicted and reported locations of z_{CHF}.

length for Run 1_1146. The overall pressure drop between stations 1 and 12 measured in the test was 27.6 kPa. The code predicted 25.9 kPa.

Fig. 16 is a parity plot of all 132 wall temperatures from the 11 Hendricks LH_2 runs modeled when the code searched for z_{CHF}. The MAPE is 34.3 %, and 82.6 % of the wall temperatures were predicted within 50 % of the measured temperatures. Most of the outliers are points along the bottom of the graph, where the wall temperature was significantly under-predicted. These points were correctly predicted in the FB regime. However, they were in the subcooled FB regime, where substitution of the superheated IAFB correlation predicts very high heat transfer coefficients and thus very low wall temperatures.

In case 1_1146, the code determined z_{CHF} to be at the inlet. In the other ten cases modeled, the critical point was found to be near the inlet by the DNB mechanism. z_{CHF} was always predicted to be less than 3 cm; the most upstream thermocouple station was at 6.35 cm, so it is not possible to compare closely the predicted z_{CHF} with test data. All the reported wall temperatures are in the FB regime.

Fig. 17 is a parity of the Hendricks runs when z_{CHF} was fixed at the

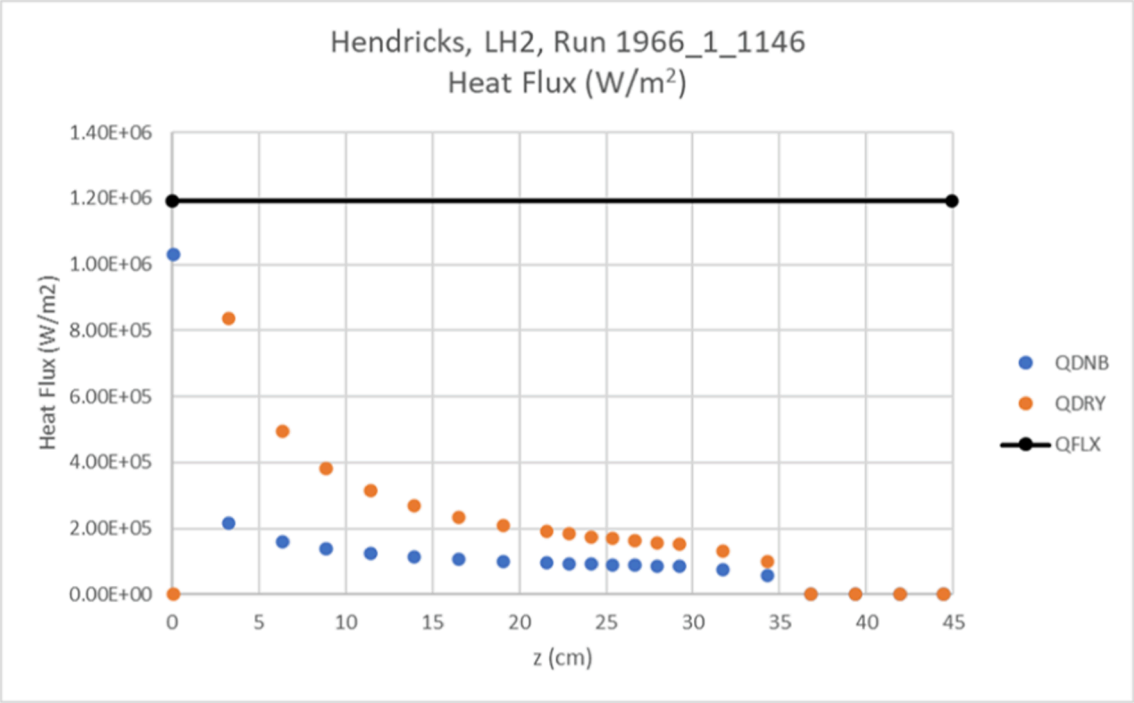

Fig. 13. Heat flux curves for Hendricks Run 1_1146.

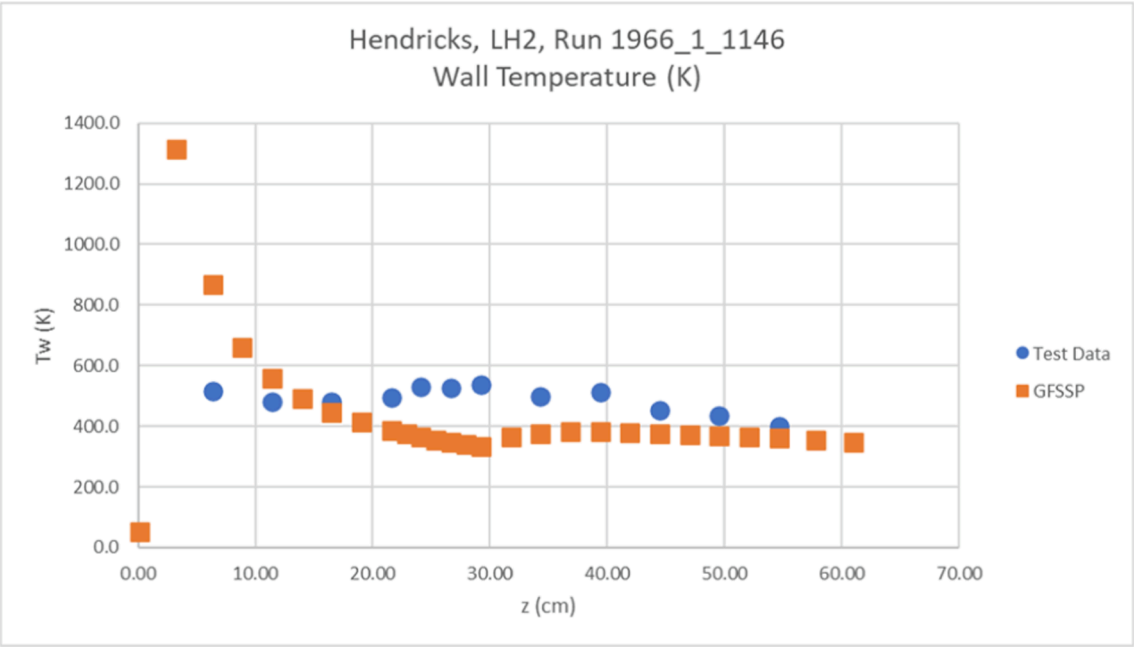

Fig. 14. Measured and predicted wall temperatures for Hendricks Run 1_1146, when the code determines z_{CHF} at the inlet.

inlet. Note that the results are almost the same as when the code finds z_{CHF}. The main difference is that, because the critical point is fixed at the inlet, the blending function was disabled.

Fig. 18 is a parity plot of the predicted and measured pressure drops between Stations 1 and 12 for the 11 modeled Hendricks runs. The MAPE is 13.8 %, and 90.9 % of the predictions fall within 30 %. The one outlier is Run 2_1247, where the measured pressure drop is 75.8 kPa and the prediction is 29.6 kPa. However, this run has an unusually large pressure drop between Stations 1 and 2 not seen in any other run. For this run, the measured pressure drop between Stations 2 and 12 is 41.4 kPa, compared to a prediction of 28.9 kPa, a much smaller error. In all 11 runs, the code logic chose the homogeneous equilibrium model to calculate the pressure drop.

4.3. Giarrantano et al. LHe (1973)

Figs. 19–20 illustrate the model output for the run plotted in Giarrantano Fig. 3.1 (hereafter called Run Fig. 3.1). For this run, the inlet pressure was 109 kPa. The mass flux was 48 kg/m^2-s, and the heat flux was 2.3 kW/m^2.

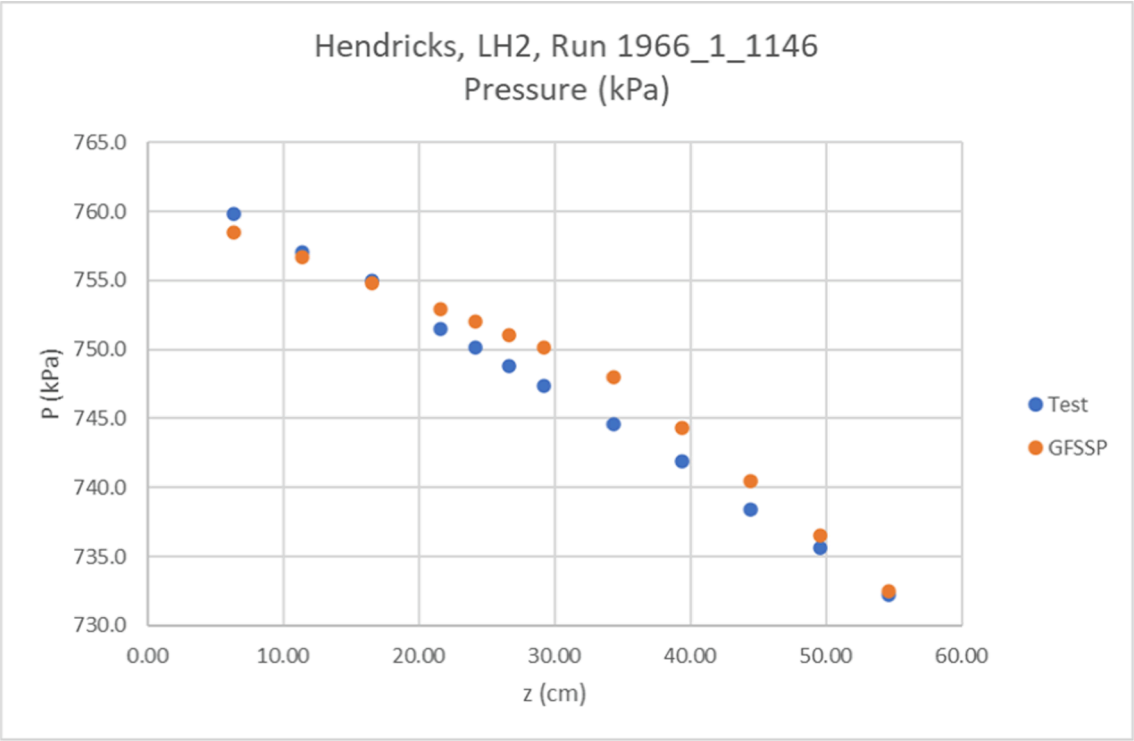

Fig. 15. Measured and predicted pressures for Hendricks Run 1_1146.

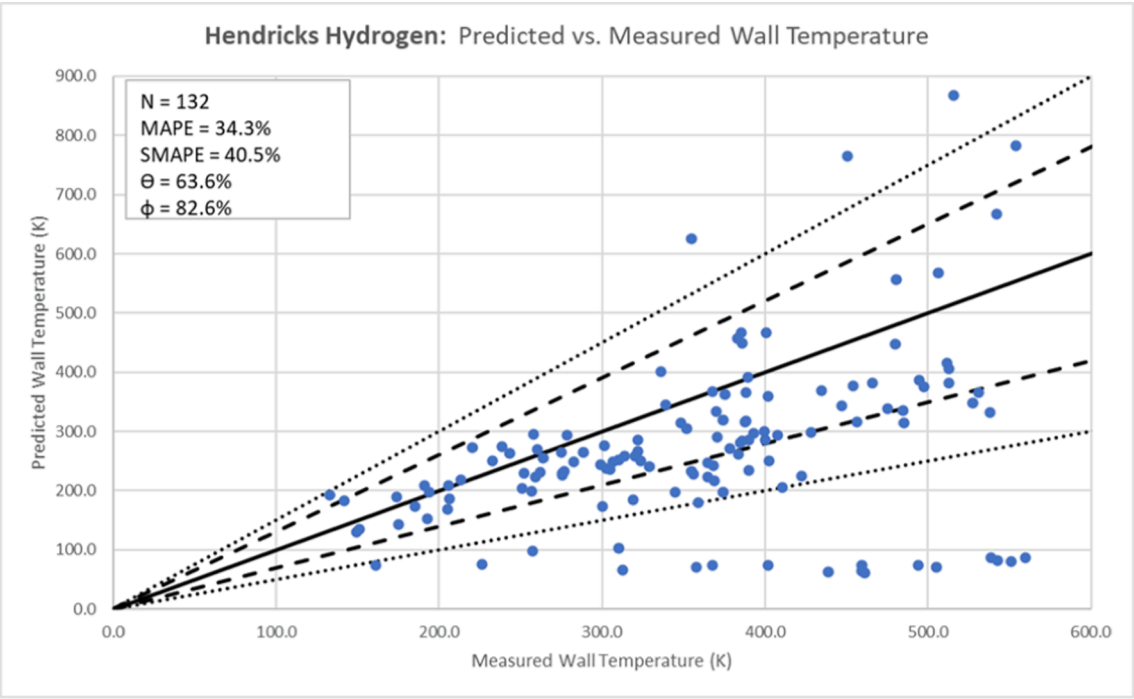

Fig. 16. Parity plot of all Hendricks LH_2 runs when code searches for z_{CHF}.

Fig. 19 plots the critical heat flux curves as functions of axial distance. Note that there is an intersection with the Q_{DNB} curve at 8 cm; however, at this location the Zivi void fraction is greater than 0.6, so it does not meet the criterion for z_{CHF}. The Q_{DRY} curve never intersects the known heat flux, so the critical point is not located, and all points are modeled in the NB regime.

Fig. 20 plots the measured and predicted wall temperatures for Giarrantano Run Fig.3.1 when the code searches for but does not locate the critical point. Wall temperatures are generally well predicted at the first eight stations. At the last two stations, which should have been in the FB regime but were evaluated in the NB regime, the wall temperatures are under-predicted.

For five of the 10 Giarrantano LHe runs, measured wall temperatures indicate a critical point in the test section. However, in only one of these

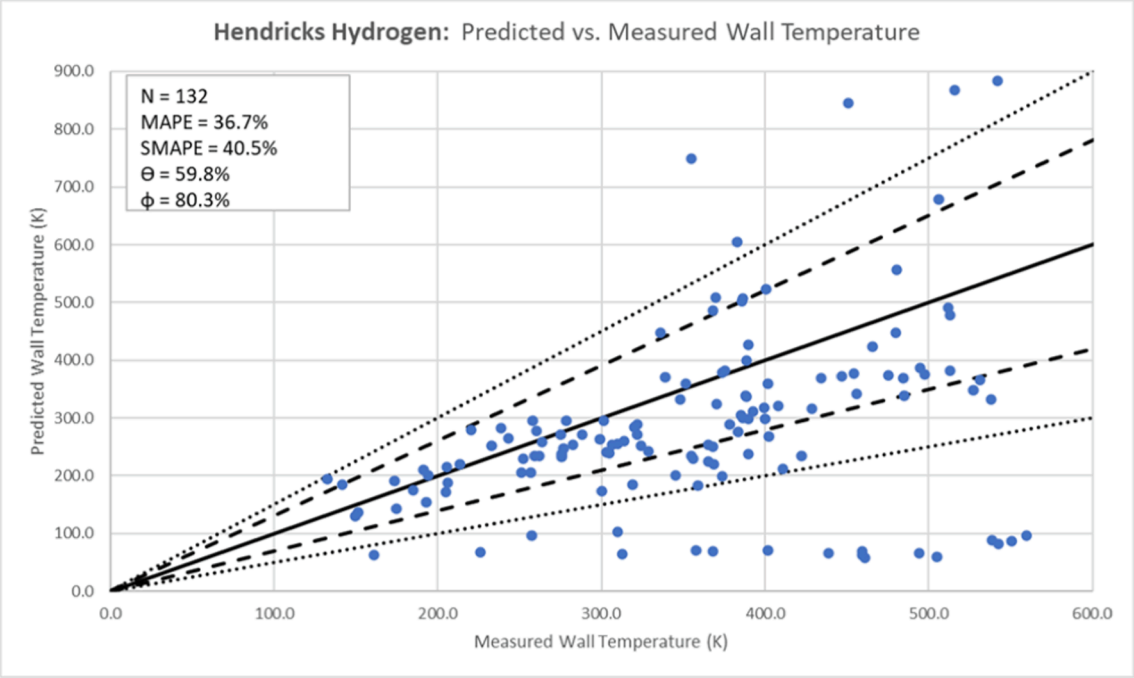

Fig. 17. Parity plot of all Hendricks LH_2 runs when z_{CHF} is fixed at the inlet.

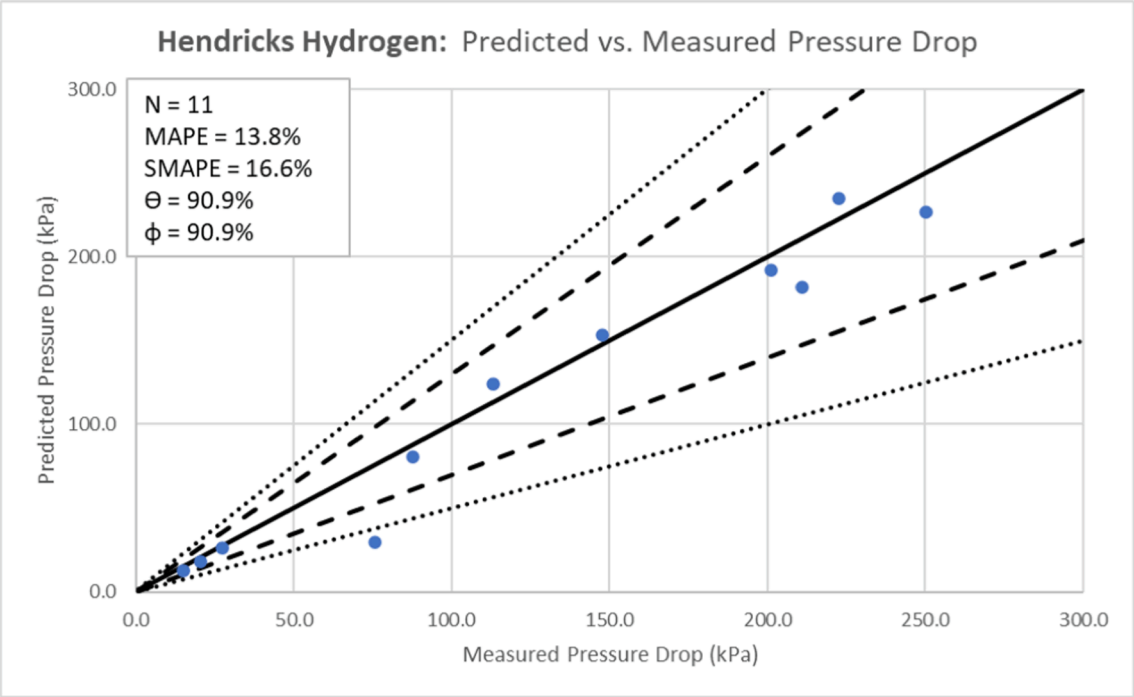

Fig. 18. Pressure drop parity plot of all Hendricks LH_2 runs.

five cases (Run Fig. 9.1) did the code locate z_{CHF}.

Fig. 21 is a parity plot of all 100 wall temperatures from the 10 Giarrantano LHe runs modeled when the code searched for z_{CHF}. The MAPE is 10.8 %, and 95 % of the wall temperatures were predicted within 50 % of the measured temperatures. The outliers on the lower right occur where the wall temperature was significantly under-predicted because they were modeled as NB instead of FB.

Fig. 22 is a parity plot of the 81 wall temperatures in the NB regime modeled when z_{CHF} was fixed at the observed location. The MAPE is 3.5 %, and 100 % of the predicted wall temperatures fall within 30 % of the measured values.

Fig. 23 is a parity plot of the 19 wall temperatures in the FB regime modeled when z_{CHF} was fixed at the observed location. The MAPE is 24.3 %, and 94.7 % of the predicted wall temperatures fall within 50 % of the measured values. It is observed that in the FB regime, the code is more likely to under-predict the wall temperatures than to over-predict.

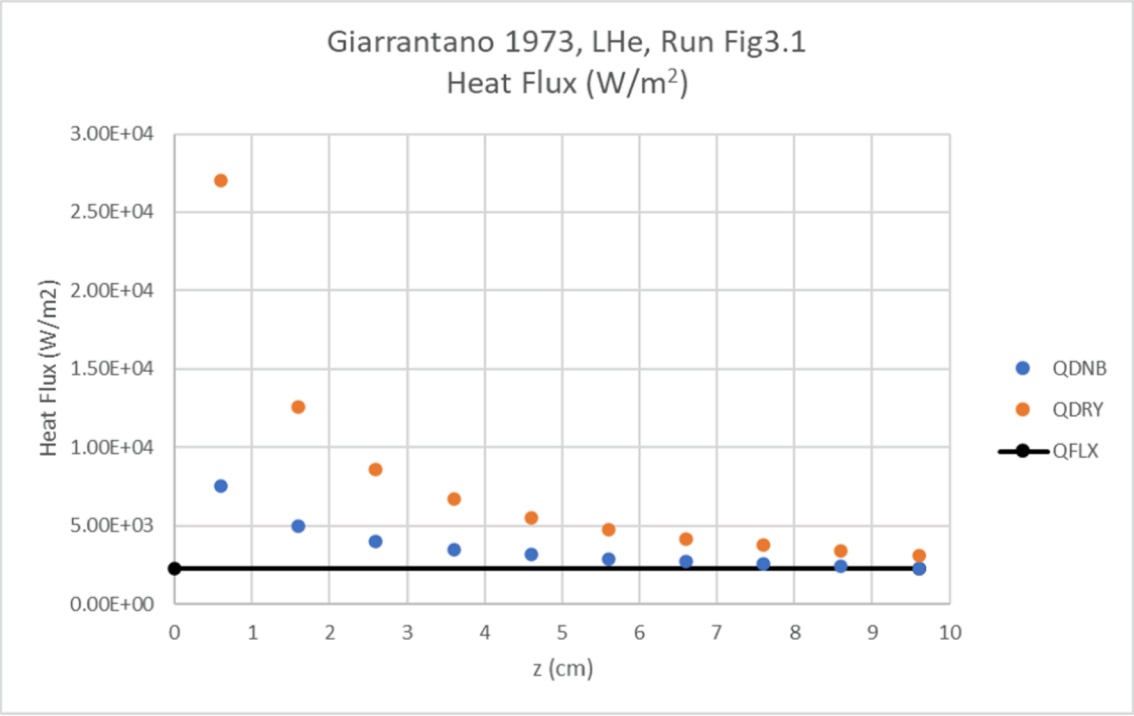

Fig. 19. Heat flux curves for Giarrantano Run Fig3.1.

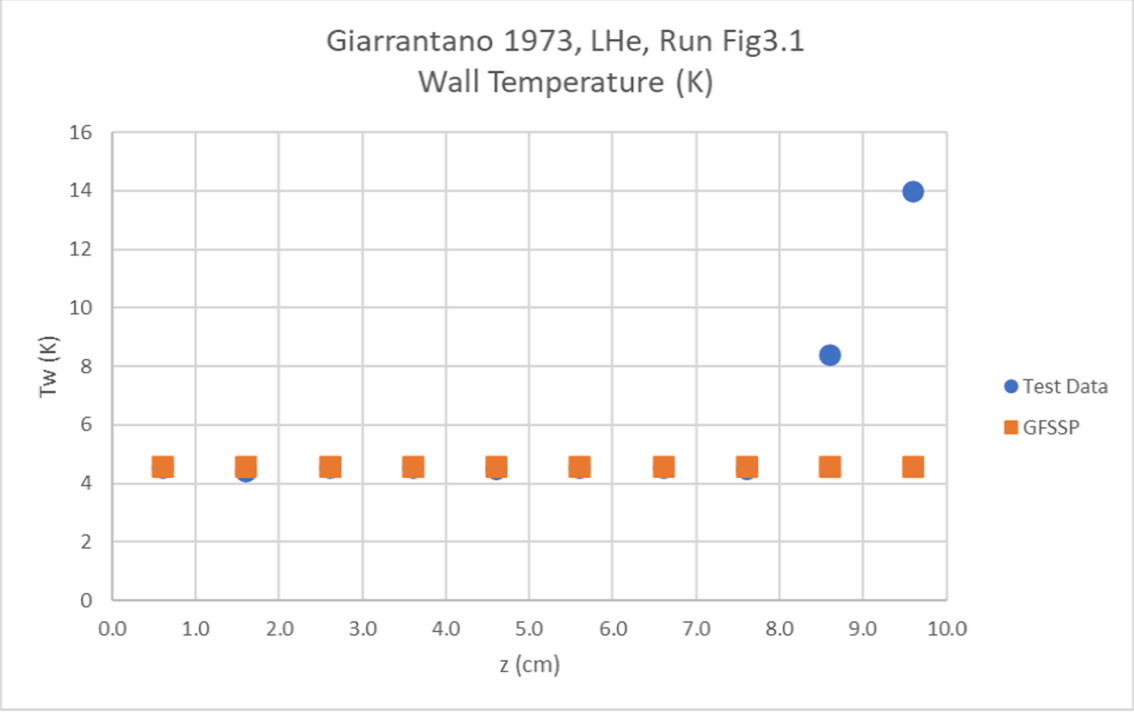

Fig. 20. Measured and predicted wall temperatures for Giarrantano Run Fig3.1, when the code searches for but does not find z_{CHF}.

5. Conclusions

Numerical models of flow boiling in heated tubes have been developed using GFSSP, a general-purpose flow network code. The models have been used to evaluate the performance of new universal cryogenic flow boiling and two-phase pressure drop correlations.

Comparison of the predicted and measured wall temperatures indicates that the model was able to locate the critical point z_{CHF} in the LH_2 cases but was less successful with the LHe cases. The algorithm was frequently unable to determine whether the mechanism for the boiling regime transition should be Departure from Nucleate Boiling or Dryout. The assumption of Dryout in ambiguous cases was successful approximately half the time, so that there is no clear benefit to changing the assumption to be DNB. Improving the criteria for distinguishing between DNB and DRY would be worthwhile forward work. In the meantime, it is recommended that in ambiguous cases, modelers assume whichever

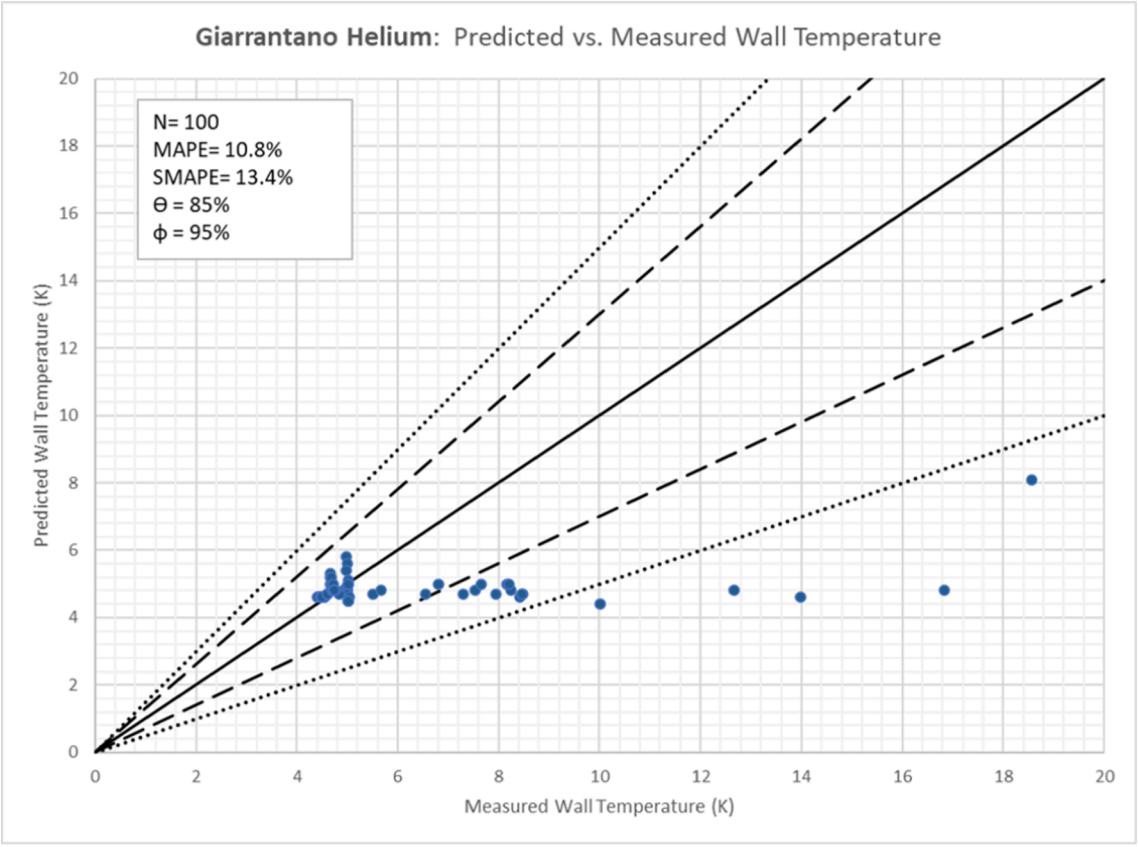

Fig. 21. Parity plot of all Giarrantano LHe runs when code searches for z_{CHF}.

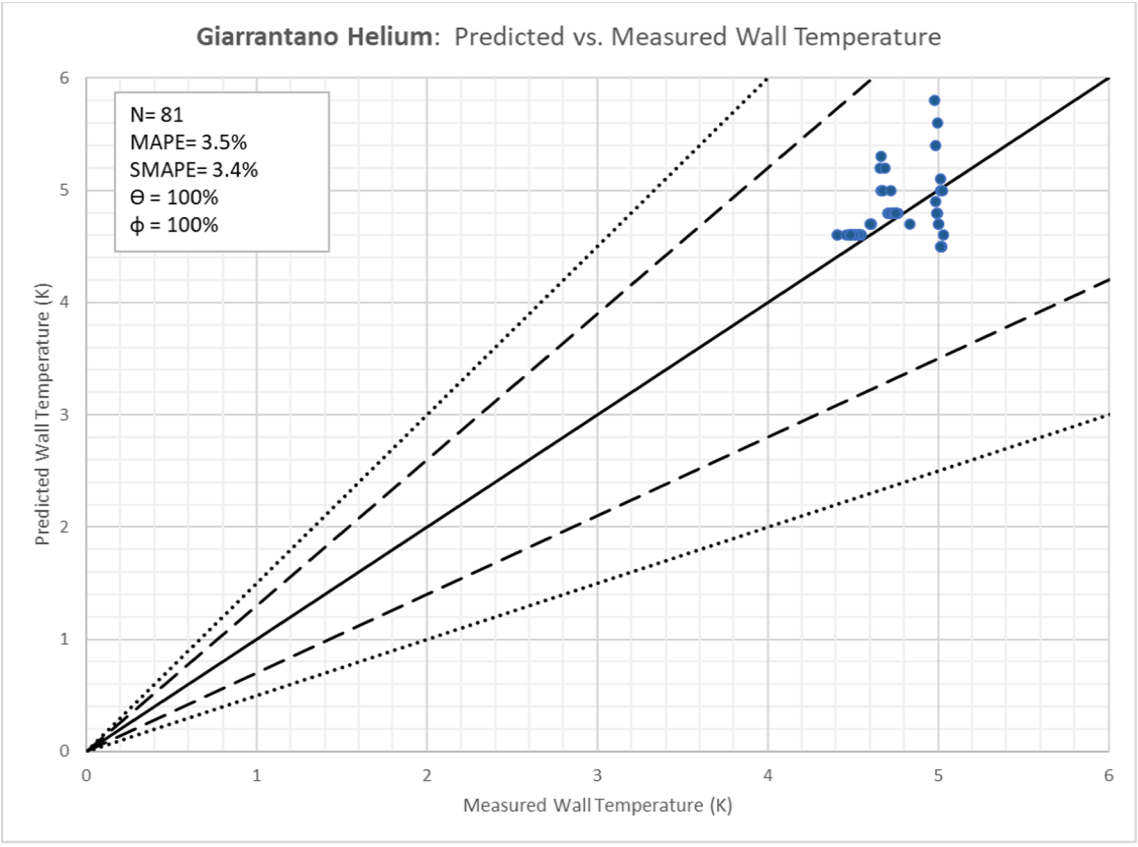

Fig. 22. Parity plot of Giarrantano LHe runs in the NB regime when z_{CHF} is fixed at the observed location.

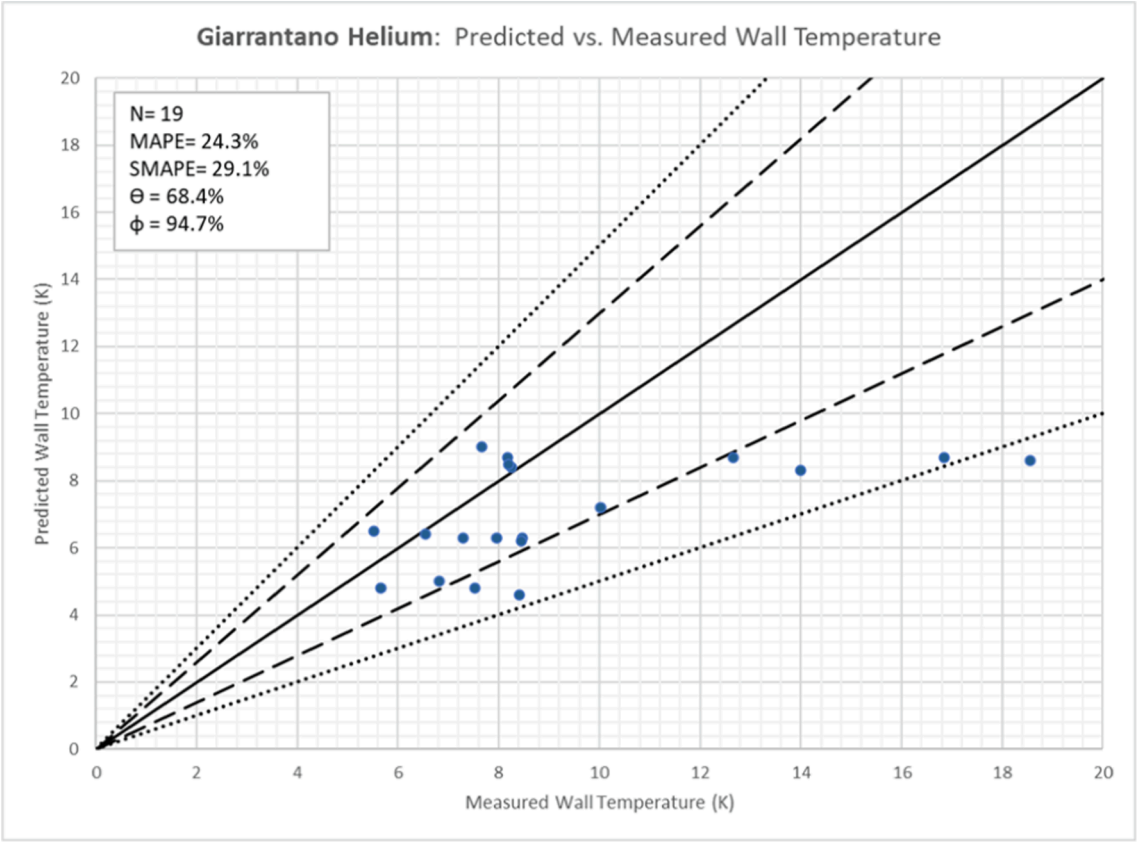

Fig. 23. Parity plot of Giarrantano LHe runs in the FB regime when z_{CHF} is fixed at the observed location.

mechanism would lead to more conservative wall temperatures for their application.

With the new universal cryogenic flow boiling correlations, in more than 60 % of cases GFSSP predicted absolute wall temperatures within the target error of 30 %. Relative errors in wall temperatures were lower in the nucleate boiling regime than in the film boiling regime. Therefore the smallest errors in wall temperature were for the Giarrantano liquid helium cases, which were predominantly in the nucleate boiling regime.

Additional forward work should include the development of a subcooled film boiling correlation, to improve the prediction of wall temperatures in cases like Hendricks et al. [20], where the inlet is subcooled and heat fluxes are high.

The new universal cryogenic flow boiling correlations are shown to model the film boiling regime more accurately than the Miropolskii [26] correlation that is the default film boiling correlation in GFSSP. When modeling experiments that were entirely in the film boiling regime, the MAPE in wall temperature was reduced by 40 % compared to modeling with Miropolskii. This makes the new correlations promising candidates for inclusion in future releases of the code.

The pressure drop correlations, which include friction, gravity, and acceleration terms, were found to model accurately the pressure drop in the Hendricks et al. LH_2 cases [20]. These cases were all modeled with the Homogeneous Equilibrium formulation of the pressure drop correlations. Additional modeling of experiments in the Separated Flow regime remains forward work.

In comparison to historical test validation cases, GFSSP with the newly implemented cryogenic flow boiling correlations yields reasonable agreement with the liquid hydrogen cases from Lewis et al. [19] and Hendricks et al. [20] and very good agreement with the liquid helium case from Giarrantano et al. [21].

CRediT authorship contribution statement

André LeClair: Writing – original draft, Software, Formal analysis. **Michael Baldwin:** Writing – review & editing, Software, Formal analysis. **Alok Majumdar:** Writing – review & editing, Software. **Jason Hartwig:** Writing – review & editing, Supervision, Project administration, Methodology, Formal analysis, Data curation. **Vishwanath Ganesan:** Writing – review & editing, Investigation, Formal analysis, Data curation. **Issam Mudawar:** Writing – review & editing, Supervision.

Declaration of competing interest

The authors declare that they have no known competing financial interests or personal relationships that could have appeared to influence the work reported in this paper.

Data availability

Data will be made available on request.

References

[1] Kim S, Mudawar I. Review of databases and predictive methods for heat transfer in condensing and boiling mini/micro-channel flows. Int J Heat Mass Transf 2014;77:627–52.
[2] Kim S, Mudawar I. Universal approach to predicting two-phase frictional pressure drop for mini/micro-channel saturated flow boiling. Int J Heat Mass Transf 2013;58:718–34.
[3] Shah M. Unified correlation for heat transfer during boiling in plain mini/micro and conventional channels. Int J Refrig 2017;74:606–26.
[4] Shah M. Comprehensive correlation for dispered flow film boiling heat transfer in mini/micro tubes. Int J Refrig 2017;78:32–46.

[5] Hartwig J, Darr S, Asencio A. Assessment of existing two phase heat transfer coefficient and critical heat flux correlations for cryogenic flow boiling in pipe quenching experiments. Int J Heat Mass Transf 2016;93:441–63.
[6] Mercado M, Wong N, Hartwig JW. Assessment of two-phase heat transfer coefficient and critical heat flux correlations for cryogenic flow boiling in pipe heating experiments. Int J Heat Mass Transf 2019;133:295–315.
[7] Darr SR, Hartwig JW, Dong J, Wang H, Majumdar AK, LeClair AC, et al. "Two-phase pipe chilldown correlations for liquid nitrogen and liquid hydrogen". ASME J Heat Mass Transf 2019;141(4):042901.
[8] LeClair A, Hartwig JW, Hauser DM, Diaz-Hyland PG, Going TR. Modeling cryogenic chilldown of a transfer line with GFSSP. *AIAA*-2018-4756, 54th Joint Propulsion Conference Cincinnati, OH, July 9–11, 2018.
[9] Sakowski B, Hauser D, Hartwig JW, Kassemi M. Validation of heat transfer correlations in line chilldown tests of cryogenic fluid in SINDA/FLUINT. AIAA-2018-4884, 54th Joint Propulsion Conference Cincinnati, OH, July 9 – 11, 2018. 2018.
[10] Wallis GB. One dimensional two-phase flow. Mcgraw-Hill; 1969.
[11] Cross MF, Majumdar AK, Bennett Jr JC, Malla RB. Modeling of chill down in cryogenic transfer lines. J Spacecr Rocket 2002;39(2):284–9.
[12] Majumdar A, Ravindran SS. Numerical modeling of conjugate heat transfer in fluid network. J Prop Power 2011;27(3):620–30.
[13] Majumdar AK, LeClair AC, Moore R, Schallhorn PA. Generalized Fluid System Simulation Program, Version 6.0. NASA/TP-2016-218218, March 2016.
[14] Ganesan V. Development of universal databases and predictive tools for two-phase heat transfer and pressure drop in cryogenic flow boiling heated tube experiments. Purdue University; 2023. Ph.D. dissertation.
[15] Ganesan V, Patel R, Hartwig JW, Mudawar I. Review of databases and correlations for saturated flow boiling heat transfer coefficient for cryogens in uniformly heated tubes, and development of new consolidated database and universal correlations. Int J Heat Mass Transf 2021;179:121656.
[16] Ganesan V, Patel R, Hartwig JW, Mudawar I. Universal critical heat flux (CHF) correlations for cryogenic flow boiling in uniformly heated tubes. Int J Heat Mass Transf 2021;166:120678.
[17] Ganesan V, Patel R, Hartwig JW, Mudawar I. Universal correlations for post-CHF saturated and superheated flow film boiling heat transfer coefficient, minimum heat flux and rewet temperature for cryogenic fluids in uniformly heated tubes. Int J Heat Mass Transf 2022;195:123054.
[18] Ganesan V, Patel R, Hartwig JW, Mudawar I. Development of two-phase frictional pressure gradient correlation for saturated cryogenic flow boiling in uniformly heated tubes. Int J Heat Mass Transf 2024;220:124901.
[19] Lewis JP, Goodykoontz JH, Kline JF. Boiling Heat Transfer to Liquid Hydrogen and Nitrogen in Forced Flow. NASA Technical Note D-1314, September 1962.
[20] Hendricks RC, et al. Experimental Heat-Transfer Results for Cryogenic Hydrogen Flowing in Tubes at Subcritical and Supercritical Pressures to 800 Pounds per Square Inch Absolute. NASA Technical Note D-3095, 1966.
[21] Giarrantano PJ, Hess RC, Jones MC. Forced Convection Heat Transfer to Subcritical Helium I. Interim Report, NBSIR 73-322, May 1973.
[22] Hartwig J, et al. A continuous flow boiling curve in the heating configuration based on new cryogenic universal correlations. Appl Therm Eng 2024;248:123235.
[23] McAdams WH, Woods WK, Heroman Jr LC. Vaporization inside horizontal tubes - II benzene-oil mixtures. J Fluids Eng, Trans ASME 1942;64:193–9.
[24] Lockhart RW, Martinelli R. Proposed correlation of data for isothermal two-phase, two-component flow in pipes. Chem Eng Prog 1949;45:39–48.
[25] Zivi SM. Estimation of steady-state steam void-fraction by means of the principle of minimum entropy production. J Heat Transfer 1964;86:247–51.
[26] Miropolski ZL. Heat transfer in film boiling of a steam-water mixture in steam generating tubes. Teploenergetika 1963;10(5):49–52.